JOURNAL OF GEOPHYSICAL RESEARCH: ATMOSPHERES, VOL. 118, 547–562, doi:10.1002/jgrd.50153, 2013

Assessment of surface winds over the Atlantic, Indian, and Pacific Ocean sectors of the Southern Ocean in CMIP5 models: historical bias, forcing response, and state dependence

Thomas J. Bracegirdle,[1] Emily Shuckburgh,[1] Jean-Baptiste Sallee,[1] Zhaomin Wang,[2] Andrew J. S. Meijers,[1] Nicolas Bruneau,[1] Tony Phillips,[1] and Laura J. Wilcox[3]

Received 13 July 2012; revised 20 December 2012; accepted 27 December 2012; published 30 January 2013.

[1] An assessment of the fifth Coupled Models Intercomparison Project (CMIP5) models' simulation of the near-surface westerly wind jet position and strength over the Atlantic, Indian and Pacific sectors of the Southern Ocean is presented. Compared with reanalysis climatologies there is an equatorward bias of 3.3° (inter-model standard deviation of ± 1.9°) in the ensemble mean position of the zonal mean jet. The ensemble mean strength is biased slightly too weak, with the largest biases over the Pacific sector (−1.4 ± 1.2 m/s, −19%). An analysis of atmosphere-only (AMIP) experiments indicates that 28% of the zonal mean position bias comes from coupling of the ocean/ice models to the atmosphere. The response to future emissions scenarios (RCP4.5 and RCP8.5) is characterized by two phases: (i) the period of most rapid ozone recovery (2000–2049) during which there is insignificant change in summer; and (ii) the period 2050–2098 during which RCP4.5 simulations show no significant change but RCP8.5 simulations show poleward shifts (0.33, 0.18 and 0.27°/decade over the Atlantic, Indian and Pacific sectors, respectively), and increases in strength (0.07, 0.08 and 0.15 m/s/decade, respectively). The models with larger equatorward position biases generally show larger poleward shifts (i.e. state dependence). This inter-model relationship is strongest over the Pacific sector ($r = -0.91$) and weakest over the Atlantic sector ($r = -0.39$). An assessment of jet structure shows that over the Atlantic sector jet shift is not clearly linked to indices of jet structure whereas over the Pacific sector the distance between the sub-polar and sub-tropical westerly jets appears to be important.

Citation: Bracegirdle, T. J., E. Shuckburgh, J.-B. Sallee, Z. Wang, A. J. S. Meijers, N. Bruneau, T. Phillips, and L. J. Wilcox (2013), Assessment of surface winds over the Atlantic, Indian, and Pacific Ocean sectors of the Southern Ocean in CMIP5 models: historical bias, forcing response, and state dependence, *J. Geophys. Res. Atmos.*, *118*, 547–562, doi:10.1002/jgrd.50153.

1. Introduction

[2] In recent decades, the climatological maximum in near-surface (10 m) westerly winds over Southern Hemisphere mid latitudes (referred to hereinafter as the 'surface jet') has shifted polewards and strengthened. Current modelling and observational evidence suggests that this is largely in response to the depletion of stratospheric ozone with an additional contribution from greenhouse gas (GHG) concentration increases [*Thompson and Solomon*, 2002; *Shindell and Schmidt*, 2004; *Arblaster and Meehl*, 2006; *Roscoe and Haigh*, 2007; *Yang et al.*, 2007]. In the ocean, the influence of these atmospheric changes has been linked to changes in sea ice, eddy kinetic energy, sea surface temperature (SST), mixed-layer depth and circulation [*Hall and Visbeck*, 2002; *Meredith and Hogg*, 2006; *Sen Gupta and England*, 2006; *Verdy et al.*, 2006; *Ciasto and Thompson*, 2008; *Sallee et al.*, 2008, 2010; *Stammerjohn et al.*, 2008; *Thompson et al.*, 2011; *Wang et al.*, 2011]. In addition, changes in the upper ocean associated with wind forcing may have had an impact on carbon uptake and storage in the Southern Ocean, both directly, through upwelling and outgassing [e.g. *Le Quere et al.*, 2007] and indirectly, by influencing nutrient cycles and phytoplankton activity [*Lovenduski and Gruber*, 2005; *Lovenduski et al.*, 2007; *Sallee et al.*, 2010]. An accurate representation of the surface westerly winds at southern mid-latitudes is therefore critical to many aspects of the coupled climate system.

[3] In terms of future projections, most of the recent and current generation of climate models exhibit a poleward shift and strengthening of the Southern Hemisphere surface jet in response to greenhouse gas (GHG) increases [*Fyfe and Saenko*, 2006; *Miller et al.*, 2006; *Bracegirdle et al.*, 2008; *Wilcox et al.*, 2013]. However, model studies including projected future ozone recovery have indicated that in austral summer (DJF) the response of the surface jet to GHG

[1]British Antarctic Survey, UK.
[2]School of Marine Sciences, Nanjing University of Information Science and Technology, China.
[3]NCAS-Climate, Department of Meteorology, University of Reading, UK.

Corresponding author: Thomas J Bracegirdle, British Antarctic Survey, High Cross, Madingley Road, Cambridge, CB3 0ET. (tjbra@bas.ac.uk)

2169-897X/13/10.1002/jgrd.50153

increases may be largely cancelled out by the response to ozone recovery during the first half of the 21st century [*Miller et al*., 2006; *Son et al*., 2010; *Arblaster et al*., 2011; *Polvani et al*., 2011]. A key advance of the climate models contributing to the recently compiled Coupled Model Intercomparison Project phase 5 (CMIP5) dataset [*Taylor et al*., 2012] is the universal inclusion of the representation of stratospheric ozone changes, which was omitted from some of the CMIP3 models. In addition, most of the CMIP3 models did not have a well-resolved stratosphere [*Karpechko et al*., 2008], whereas the CMIP5 ensemble includes a number of so-called "high top" models with an upper boundary at or above 1 hPa. In addition, 12 of the CMIP5 models have a latitudinal grid spacing in the atmosphere of 1.5° or less (see Table 1) compared with only two of the CMIP3 models [*Maloney and Chelton*, 2006]; increased latitudinal resolution has been linked in some modelling studies to reductions in the climatological position bias of the surface jet [*Guemas and Codron*, 2011; *Hourdin et al*., 2012]. These three developments make the CMIP5 ensemble of models more suitable than earlier generations for assessing the response of the Southern Hemisphere jet to future climate change scenarios.

[4] The focus of this study is on the projections of surface winds, for which variations in present-day climatology and projected change are of great importance in understanding impacts on, and interactions with, the ocean. While a number of studies have focussed on the response of zonal mean tropospheric winds in coupled climate models [e.g. *Wilcox et al*., 2013], here we assess the Atlantic, Indian and Pacific sectors individually. We are motivated to do this for two reasons. The first is that it is important to understand the longitudinal differences to assess the impact of the surface winds on the ocean, and in particular on carbon uptake [*Sallee et al*., 2010]. The second is that different mechanisms may contribute to changes in the surface jet in different sectors. For example, the atmospheric wave breaking characteristics vary zonally [*Wang and Magnusdottir*, 2011; *Barnes and Hartmann*, 2012], which is in part a consequence of the longitudinal variations in orography associated with South America and South Africa [*Inatsu and Hoskins*, 2004]. From a storm-track perspective, a major cyclogenesis region over the orography of South America triggers baroclinic eddies that follow a spiral track around the whole Southern Ocean towards Antarctica in the Pacific sector [*Hoskins and Hodges*, 2005]. A secondary smaller genesis region over Australia and New Zealand feeds into the Pacific storm track. This is partially reflected in the time-mean westerly wind field, which shows a maximum at lower latitudes in the Pacific compared to the Atlantic (Figure 1). These zonal asymmetries in the storm track are much more pronounced in winter and are thought to be

Table 1. CMIP5 Model Details[a]

(Model number) Model Name	Historical Run Numbers (ua; uas; ta)	RCP4.5 Run Numbers (uas)	RCP8.5 Run Numbers (uas; ta)	Vertical Levels (model top)	Latitudinal Grid Spacing	Ozone
(1) ACCESS1.0*	1;1;1	1	1;1	38 (4 hPa)	1.25°	P^{CS}
(2) ACCESS1.3*	1;1;1	1	1;1	38 (4 hPa)	1.25°	P^{CS}
(3) BCC-CSM1.1	1–3;1–3;1–3	1	1;1	26 (2.9 hPa)	2.8°	P^{C}
(4) BCC-CSM1.1(m)	1–3;1–3;1	1	1;1	26 (2.9 hPa)	1.0°	P^{C}
(5) BNU-ESM*	1;1;1	1	1;1	26 (2.9 hPa)	2.8°	O
(6) CanESM2	1–5;1–5;1	1–5	1–5;1–5	**35 (1 hPa)**	2.8°	P^{LR}
(7) CMCC-CM*	1;1;1	1	1;1	31 (10 hPa)	0.75°	P^{CS}
(8) CMCC-CMS	1;1;1	1	1;1	**95 (0.01 hPa)**	1.8°	P^{CS}
(9) CNRM-CM5*	2–9; 2–9; 2–9	1	1–2,4,6,10; 2,4,6,10	31 (10 hPa)	1.4°	I
(10) CSIRO-Mk3.6.0*	1–10; 1–10; 1–10	1–10	1–10; 1–10	18 (4.52 hPa)	1.9°	P^{C}
(11) FGOALS-s2*	1–3;1–3;1	2–3	1–3;1	26 (2.2 hPa)	1.7°	P^{C}
(12) GFDL-CM3	1–5;1–5;1–5	1	1;1	**48 (1 hPa)**	1.8°	I
(13) GFDL-ESM2G	1;1;1	1	1;1	24 (3 hPa)	2.0°	P^{C}
(14) GFDL-ESM2M	1;1;1	1	1;1	24 (3 hPa)	2.0°	P^{C}
(15) GISS-E2-H (p1)	1–5;1–5;1–5	1–5	1;1	**40 (0.1 hPa)**	2.0°	$P^{RW\text{-}L}$
(16) GISS-E2-R (p1)*	1–6; 1–6; 1–6	1–6	1; 1	**40 (0.1 hPa)**	2.0°	$P^{RW\text{-}L}$
(17) HadGEM2-CC	1; 1–3; 1–3	1	1; 1–3	**60 (0.006 hPa)**	1.25°	P^{CS}
(18) HadGEM2-ES/A*	1–4; 1–4; 1–4	1–4	2; 1–4	38 (4 hPa)	1.25°	P^{CS}
(19) INM-CM4*	1; 1; 1	1	1; 1	21 (10 hPa)	1.5°	P^{C}
(20) IPSL-CM5A-LR*	1–4; 1–4; 1–4	1–4	1–4; 1–4	**39 (0.04 hPa)**	1.9°	O
(21) IPSL-CM5A-MR*	1–2; 1; 1	1	1; 1	**39 (0.04 hPa)**	1.3°	O
(22) IPSL-CM5B-LR*	1; 1; 1	1	1; 1	**39 (0.04 hPa)**	1.3°	O
(23) MIROC-ESM	1–3; 1–3; 1–3	1	1; 1	**80 (0.0036 hPa)**	2.8°	P^{K}
(24) MIROC-ESM-CHEM	1; 1; 1	1	1; 1	**80 (0.0036 hPa)**	2.8°	I
(25) MIROC5*	1; 1–4; 1–4	1–3	1–3; 1–3	56 (3 hPa)	1.4°	P^{K}
(26) MPI-ESM-LR*	1–3; 1–3; 1–3	1–3	1–3; 1–3	**47 (0.01 hPa)**	1.9°	P^{CS}
(27) MPI-ESM-MR*	1–3; 1–3; 1–3	1–3	1; 1	**95 (0.01 hPa)**	1.8°	P^{CS}
(28) MRI-CGCM3*	1–5; 1–5; 1–5	1	1; 1	**48 (.01 hPa)**	1.1°	P^{CS}
(29) NorESM1-M*	1–3; 1–3; 1–3	1	1; 1	26 (2.9 hPa)	1.9°	P^{L}

[a]Here those in bold are classified as high top models (with model tops at or above 1 hPa). Asterisks indicate the subset of 18 models used in the AMIP / historical comparisons. The different realization ("run") numbers are shown in the 2nd, 3rd and 4th columns. For the stratospheric ozone representation "I", "P" and "O" denote interactive, prescribed and offline chemistry climate model, respectively. The different prescribed datasets are indicated by the following superscripts: (i) C denotes *Cionni et al*. [2011]. (ii) CS denotes *Cionni et al*. [2011] with a solar cycle added in the future. (iii) RW-L denotes *Randel and Wu* [2007] up to 1997, constant between 1997 and 2003 then linear increase to 1979 concentration by 2050. (iv) L denotes *Lamarque et al*. [2011]. (v) K denotes *Kawase et al*. [2011]. (vi) LR denotes future stratospheric concentrations determined by combining two terms in a multiple linear regression analysis.

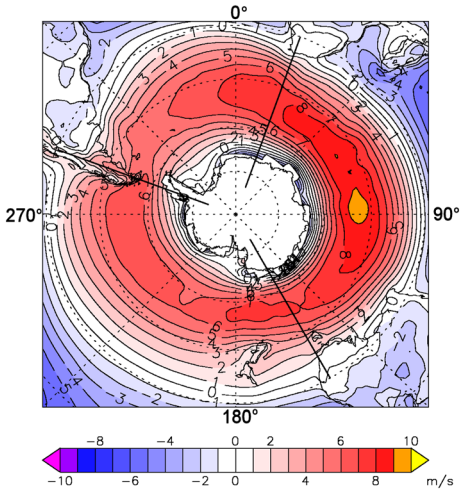

Figure 1. Climatological annual mean westerly 10 m wind from ERA-Interim for the period 1979–2010. The solid straight lines indicate the divisions between the Atlantic, Indian and Pacific sectors. The sectors are defined by longitude ranges as follows: Atlantic sector (290°–20°), Indian sector (20°–150°) and Pacific sector (150°–290°).

caused in part by asymmetries in tropical SSTs and consequent forcing [*Inatsu and Hoskins*, 2004]. Local forcing is also a major contributor to zonal asymmetries, for example the maximum in time mean zonal wind over the Indian sector (see Figure 1) is largely caused by a local maximum in the pole-to-equator SST gradient [*Inatsu and Hoskins*, 2004; *Hoskins and Hodges*, 2005].

[5] In this study we assess present-day skill and projected changes simulated by the CMIP5 models. As part of this assessment we address the question of whether the skill and projected changes in models with a good representation of the stratosphere differs from those with a relatively poorly resolved stratosphere. We also examine whether there is a 'state dependence' in the model responses, following a number of recent studies which have found that climate models with a larger poleward shift in response to GHG increases generally exhibit a larger equatorward bias in their present-day mean state [*Kidston and Gerber*, 2010; *Son et al*., 2010]. In particular the theoretical implications of differences in state dependence characteristics across different ocean sectors are investigated.

[6] This paper is structured as follows. In the next section (Section 2) the model and reanalysis datasets are described. In Section 3 the results are presented followed by discussion and conclusions in Section 4.

2. CMIP5 Model Data and Jet Diagnostics

[7] Data from the CMIP5 models were assessed in this study. Throughout this study we quote the inter-model spread of the results, however we note that some of the models included in the study are very similar (e.g. the IPSL-CM5A-LR and IPSL-CM5A-MR models differ predominantly only in their horizontal grid). The required variables were downloaded from the CMIP5 data archive. These are: westerly wind on pressure levels ("ua"), 10-metre westerly wind ("uas") and temperature on pressure levels ("ta"). The CMIP5 simulations and forcing scenarios used are shown in Table 1. In general more than one realization is available for a given model and a given scenario (i.e. the same model is run more than once with the same forcing). Where more than one realization is available (indicated in Table 1), the mean of those realizations is used. Before analysis the climate model and reanalysis data were bi-linearly interpolated onto the HadGEM2-ES horizontal grid (1.875° longitude 1.25° latitude) to allow direct comparison.

[8] The jet strength is defined as the climatological maximum in the zonal mean 10 m westerly wind component in the Southern Hemisphere and the jet position is defined as the latitude of this maximum. A cubic spline interpolation is used to quantify the maximum and determine its latitude from the gridded data. In addition to zonal mean diagnostics, ocean sectors are assessed separately. The sectors are defined by longitude ranges as follows: Atlantic sector (290°–20°), Indian sector (20°–150°) and Pacific sector (150°–290°), which are indicated in Figure 1.

[9] For comparisons to reanalysis datasets, data from the "historical" forcing simulations were used. The historical simulations are fully coupled experiments that are forced by observed 20th century variations of important climate drivers such as GHGs, ozone, aerosols and solar variability. For assessments of future change, two scenarios were assessed: Representative Concentration Pathway (RCP) 4.5 and RCP 8.5, for which the numbers refer to approximate estimates of radiative forcing at the year 2100. RCP4.5 is a medium mitigation scenario and RCP8.5 is a high emissions scenario. A full range of anthropogenic climate drivers are included in the RCP scenarios (GHGs, aerosols, chemically active gases and land use) along with a repeating 11-year solar cycle (repeating solar cycle 23), which are detailed in *Meinshausen et al*. [2011]. Recommended pathways for both concentration and emissions of GHGs are provided, since both atmosphere-ocean general circulation models and Earth system models (ESMs) are included in CMIP5.

[10] The CMIP5 models assessed here include representations of stratospheric ozone changes across both the historical and RCP scenarios. However, only seven follow the recommended time series of *Cionni et al*. [2011] and the others are based on a range of different methods and datasets, which are listed in Table 1. *Wilcox et al*. [2013, submitted to JGR-Atmospheres] show that the ozone concentrations above Antarctica qualitatively follow the changes seen in the *Cionni et al*. [2011] time series, but with a relatively large spread in absolute concentrations and differences in the rate of 21st century recovery.

[11] The observationally constrained European Centre for Medium Range Weather Forecasts (ECMWF) ERA-Interim reanalysis dataset [*Dee et al*., 2011] was used to assess the skill of the models at reproducing present-day climate. Recent studies have found ERA-Interim to be the most reliable reanalysis over Antarctica [*Bromwich et al*., 2011; *Bracegirdle and Marshall*, 2012]. Over the Southern Ocean there are few observations and some uncertainty over the comparative accuracy of near-surface wind datasets, but with indications that ERA-Interim is the most reliable of contemporary reanalyses [*Kent et al*., 2013; *Swart and Fyfe*, 2012]. We also compared the results with those derived from other recent reanalyses, NCEP Climate Forecast System Reanalysis (CFSR) [*Saha et al*., 2010] and the NASA Modern Era Retrospective-Analysis for Research and

Applications (MERRA) [*Rienecker et al.*, 2011]. This gives a measure of the uncertainty in estimates of the actual wind that is probably a slight underestimate of the true observational uncertainty [*Kent et al.*, 2013].

[12] Assessment of the skill of the atmospheric component of the CMIP5 models included a comparison between ERA-Interim and the "AMIP" atmosphere-only CMIP5 simulations. In the AMIP simulations, SST and sea ice concentration are specified based on monthly observations [*Hurrell et al.*, 2008]. For use as boundary conditions the monthly mean SST data are interpolated to daily values [*Taylor et al.*, 2000]. In all other respects (such as GHG and ozone concentrations) the AMIP runs are the same as the historical coupled runs.

3. Results

3.1. Mean State Skill

[13] The climatological zonal mean annual mean westerly 10 m wind from historical CMIP5 model runs is shown in Figure 2a. Compared with ERA-Interim, the ensemble mean position of the surface jet in the CMIP5 models shows an equatorward bias of $3.3 \pm 1.9°$ in latitude (where the range shown is the inter-model standard deviation). Every ensemble member shows an equatorward bias, ranging from 0.4° in NorESM1-M to 7.7° in IPSL-CM5A-LR. There is a large spread in climatological jet strength in the models, with values ranging from 5.0 to 9.7 $m\,s^{-1}$. The weak negative ensemble mean strength bias of $-0.4 \pm 1.0\,m\,s^{-1}$ is small compared with the inter-model standard deviation. The skill of the models in reproducing observed position and strength varies: for example, the NorESM1-M model is the most accurate in terms of position but shows the second largest positive strength bias.

[14] For ocean-atmosphere interactions it is important to consider how wind biases are distributed across the different ocean basins; this is also useful to help elucidate the processes leading to the biases. From Figure 2b–d it is clear that the characteristics of position and strength vary across different sectors of the Southern Ocean. The most notable feature is the contrast between large equatorward biases in surface jet position over the Indian ($3.4 \pm 1.6°$) and Pacific ($3.3 \pm 2.7°$) sectors (Figures 2c and 2d, respectively) and a small bias over the Atlantic sector ($1.4 \pm 1.5°$). Despite the large position bias over the Indian sector, the ensemble mean jet strength agrees closely with ERA-Interim (bias of $0.1 \pm 1.0\,m\,s^{-1}$). Agreement in jet strength is also good over the Atlantic sector (bias of $0.3 \pm 1.0\,m\,s^{-1}$), however it is too weak over the Pacific sector (bias of $-1.4 \pm 1.2\,m\,s^{-1}$). Other recently produced reanalysis datasets (MERRA and CFSR) show results in very good agreement with those based on ERA-Interim (Figure 2). Even taking into account the fact that the observational uncertainties are probably larger than the inter-reanalysis differences shown here [*Kent et al.*, 2013], it is clear that the inter-CMIP5 differences dominate the comparisons.

3.2. Relative Skill of Coupled and Atmosphere-Only Simulations

[15] The surface jet is associated with the mid-latitude storm track, which is driven by baroclinic eddies. Many factors, both local and remote, can exert an influence on the

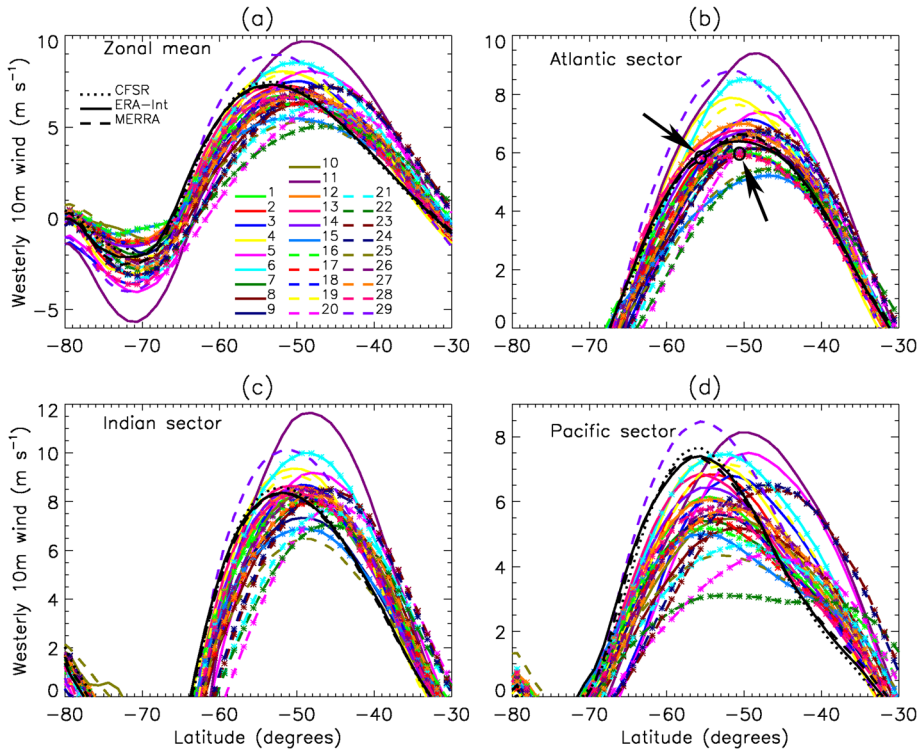

Figure 2. (a) Zonal mean annual mean 10 m westerly wind climatology for the period 1985–2004 as a function of latitude. (b), (c) and (d) show the same but for the Atlantic, Indian and Pacific sectors, respectively (note the different scales on the y axes). The colored solid and dashed lines indicate the CMIP5 models with overlaid star symbols indicating high-top models. The black solid, dotted and dashed lines show output from ERA-Interim, CFSR and MERRA, respectively. The arrows indicate double maxima exhibited by model 28 (MRI-CGCM3).

climatological location and strength of the baroclinic eddies and the associated jet. Thus determining what aspects of the coupled models might lead to the biases in the surface jet is not straightforward, particularly in a coupled modelling framework.

[16] To investigate the importance of lower boundary effects in influencing surface jet biases we compared the results from the atmosphere-only (AMIP) simulations of the CMIP5 models with the coupled simulations for the "historical" scenario. In general the AMIP simulations show greater skill in reproducing the observed surface jet position when compared with the coupled "historical" simulations (Figure 3). For the subset of 18 AMIP simulations available at time of writing, the ensemble mean equatorward bias of

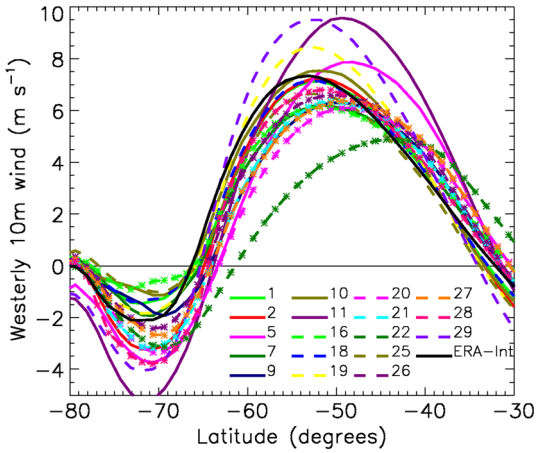

Figure 3. Data from atmosphere-only (AMIP) simulations showing zonal mean annual mean 10 m westerly wind climatology for the period 1985–2004. Following Figure 2, the colored solid and dashed lines indicate the AMIP models with overlaid star symbols indicating high top models. The black solid line shows output from ERA-Interim.

the annual mean climatological surface jet is 28% smaller than for the corresponding coupled historical simulations (2.4° compared with 3.4°) (Figure 4a). The standard deviation of the inter-model spread is also smaller, 1.9° compared with 2.2°. However, the reduction in position bias in the AMIP simulations is much greater in some models than others (Figure 4a) and notably increases in model 22 (IPSL-CM5B-LR). As might be expected, the largest and most significant differences between the AMIP and historical simulations occur over the Indian and Pacific sectors, where the historical equatorward biases are large and significant (Table 2). Here, the ensemble mean AMIP biases are 21% and 31% smaller, respectively. In terms of the surface jet strength, the differences between AMIP and historical simulations are generally smaller (Figure 4b). The only sector with a significant historical strength bias is the Pacific sector and here the AMIP simulations also exhibit a smaller difference (20% reduction in bias) compared to jet position (Table 2). The most accurate of the AMIP simulations in terms of jet strength is HadGEM2-A, with a root mean squared bias of zonal mean westerly wind of 0.7 m s^{-1} (for grid-points between 80°S and 30°S).

3.3. Changes During the 20th and 21st Century in the Zonal-Mean and in the Atlantic, Pacific and Indian Ocean Sectors

[17] In most of the CMIP5 models the zonal mean annual mean surface jet changes significantly over the period 1900 to 2100 (Figure 5, for which the historical and RCP8.5 simulations were joined to create a continuous time series). Most models show a poleward shift and all models show a strengthening of the surface jet from the late 20th century and through the 21st century following the RCP8.5 scenario. However, in some models, the changes are small and insignificant. There is no clear change in the width of the surface jet in any of the models (dashed lines in Figure 5).

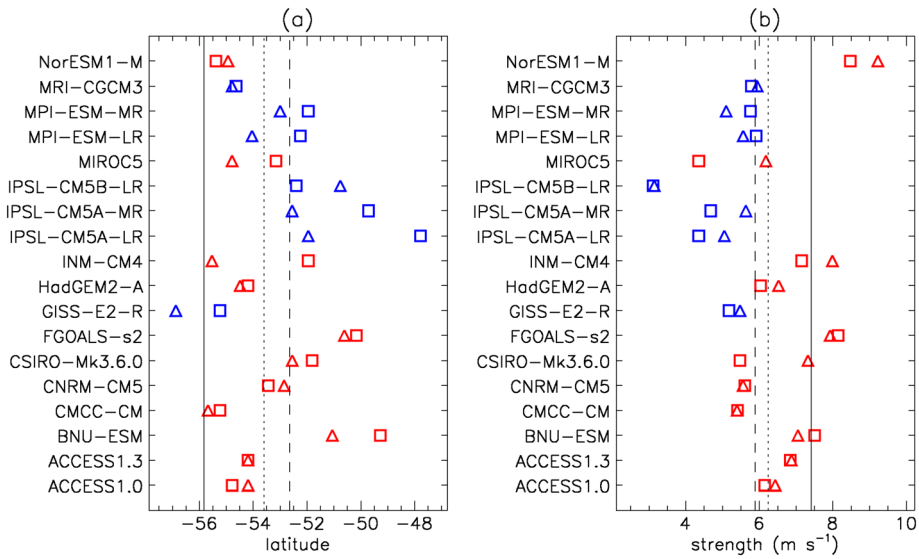

Figure 4. The surface jet position (a) and strength (b) in the subset of 18 AMIP simulations (triangles) and in the fully coupled historical simulations of the same models (squares). High top models are shown in blue and low top in red. The period 1985–2004 was used for calculations. The dashed line shows the mean of the coupled simulations, the dotted line shows the mean of AMIP simulations and the solid line shows the value derived from ERA-Interim.

Table 2. Mean and Inter-model Standard Deviation of Biases in Jet Position and Strength for the Subset of 18 AMIP Models and the Corresponding Coupled "Historical" Simulations[a]

	Zonal Mean	Atlantic Sector	Indian Sector	Pacific Sector
Historical position bias (degrees)	3.4 ± 1.9	1.4 ± 1.6	3.3 ± 1.6	3.2 ± 2.3
	[3.3 ± 1.9]	[1.4 ± 1.5]	[3.4 ± 1.6]	[3.3 ± 2.7]
AMIP position bias (degrees)	2.4 ± 2.2	0.7 ± 2.3	2.6 ± 2.3	2.2 ± 1.8
Historical strength bias ($m\,s^{-1}$)	-0.5 ± 1.2	0.3 ± 1.1	0.0 ± 1.2	-1.5 ± 1.4
	[−0.4 ± 1.0]	[0.3 ± 1.0]	[0.1 ± 1.0]	[−1.4 ± 1.2]
AMIP strength bias ($m\,s^{-1}$)	-0.3 ± 1.2	0.4 ± 1.1	0.1 ± 1.1	-1.2 ± 1.4

[a]Here differences are for annual mean climatologies over the period 1985–2004 defined relative to ERA-Interim. For reference the equivalent diagnostics for all 29 coupled CMIP5 models are shown in square brackets.

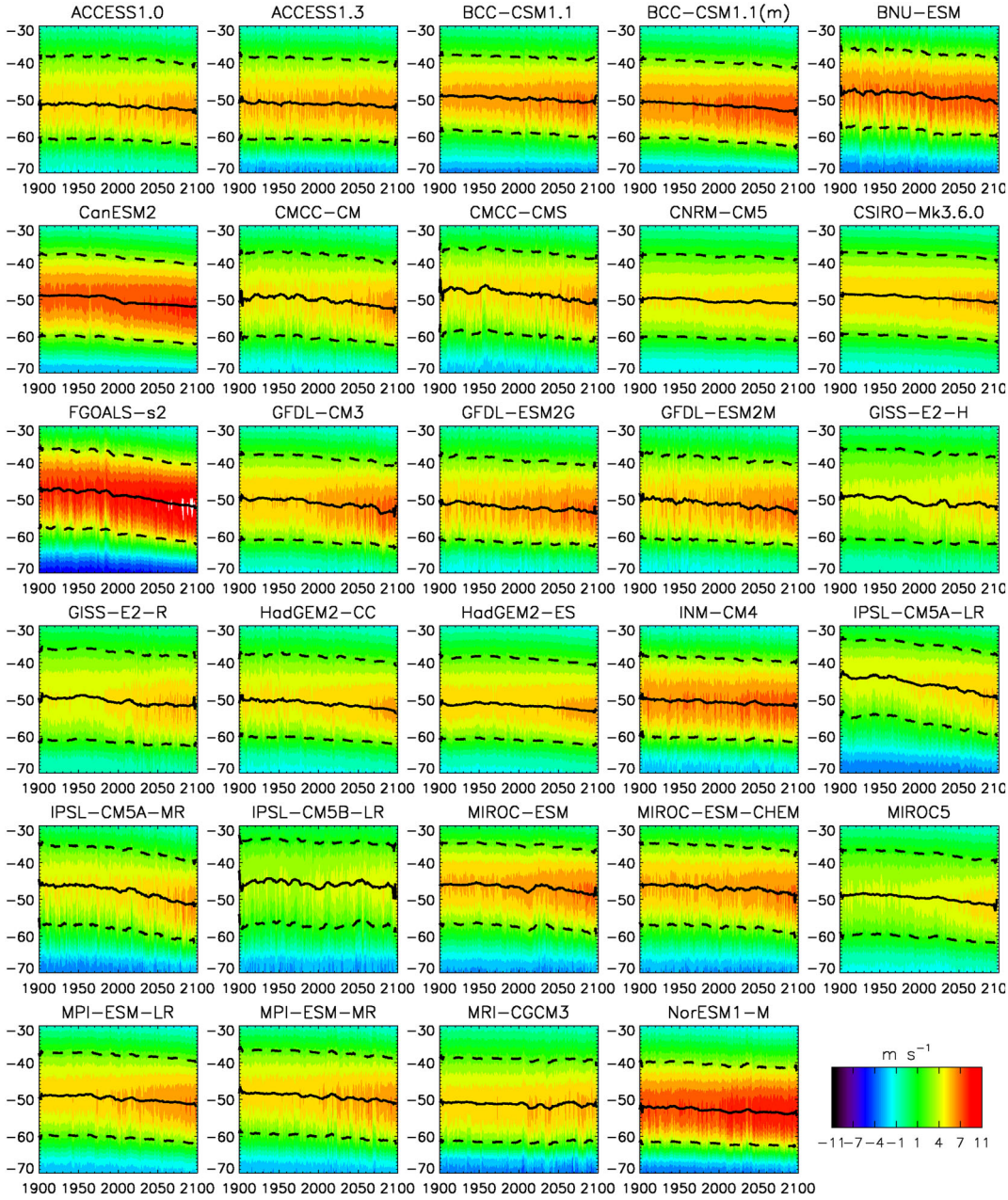

Figure 5. Latitude/time plots of annual mean zonal mean 10 m westerly wind between 1900 and 2099. The historical simulations are used up to 2005 and the RCP8.5 simulations are used from 2006 to 2099. For each model the mean of all available ensemble members is used. The solid line shows the latitude of the maximum. The dashed lines show the latitudes where the values are half of the maximum. The lines are smoothed using a 10-year moving average.

[18] The ensemble mean shifts in surface jet latitude are shown in Figure 6 for RCP4.5 and RCP8.5. Three main phases are seen in jet position shift. First, during the period of ozone depletion from the 1960s to ~2000 [*Cionni et al*., 2011] the annual mean jet position exhibits a poleward shift across all three sectors (Figure 6a,d). The 1960–1999 linear trends range from 0.18° decade^{-1} over the Indian sector to 0.27° decade^{-1} over the Atlantic sector, with a large but not statistically significant trend of 0.30° decade^{-1} over the Pacific sector (Figure 7a). Then, in the second phase, this shift in annual mean jet latitude is reduced in the first half of the 21st century in both RCP4.5 and RCP8.5 (Figures 6 and 7), during the period of most rapid simulated recovery of stratospheric ozone. Finally in the third phase, after approximately 2050 there is a large divergence between the jet shifts of the scenarios, with RCP4.5 still showing little change and RCP8.5 showing large and significant poleward shifts ranging from 0.18° decade^{-1} over the Indian sector to 0.33° decade^{-1} over the Atlantic sector (Figures 6 and 7). In summer (DJF) (Figures 6b, e and 7) the jet shifts are qualitatively similar to the annual mean, with a halt in significant poleward shift that coincides with the simulated period of stratospheric ozone recovery in the future scenarios. A similar summer cancellation between the effects of GHG increases and ozone recovery is evident in previous studies of other climate models and model inter-comparisons [*Son et al*., 2010; *Polvani et al*., 2011; *Arblaster et al*., 2011] and is seen in other jet position diagnostics of the CMIP5 models [*Wilcox et al*., 2013]. In winter (JJA) (Figure 6c,f) the shifts broadly reflect changes in radiative forcing in the

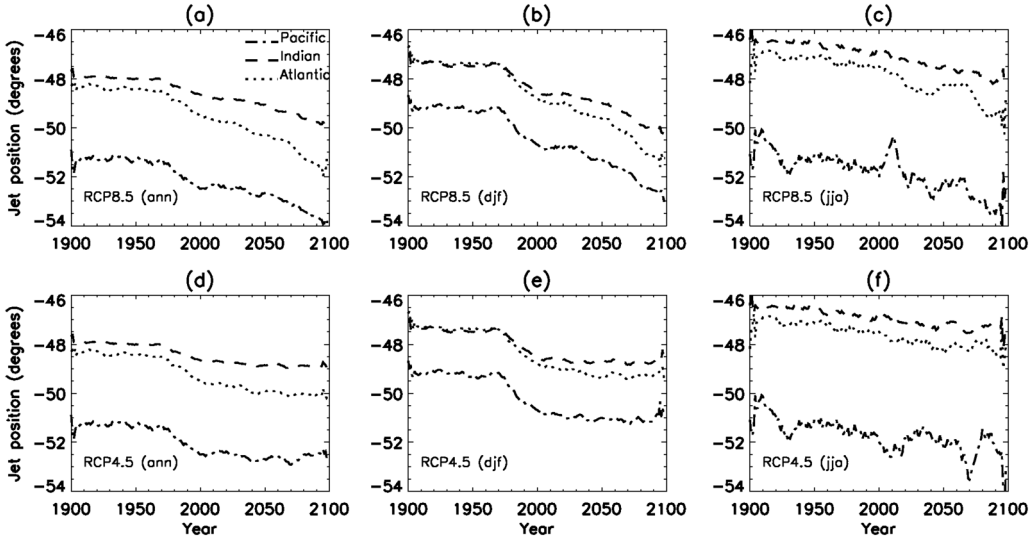

Figure 6. Time series of the latitude of the Southern Hemisphere surface jet. The period 1900–2005 is taken from historical simulations and the period 2006–2099 is taken from future scenarios RCP8.5 (a–c) and RCP4.5 (d–f). Ensemble means are shown for the Atlantic sector (dotted lines), Indian sector (dashed lines) and Pacific sector (dashed-dotted lines). Annual mean (a, d), summer (December–February) (b, e) and winter (June–August) (c, f) values are shown. The lines are smoothed using a 10-year moving average.

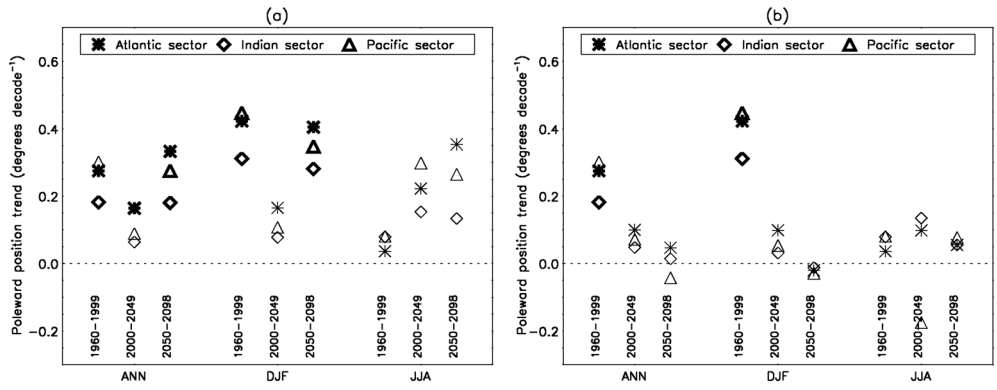

Figure 7. Linear ensemble mean poleward trends in position with the model projections based on (a) the RCP8.5 scenario and (b) the RCP4.5 scenario for annual mean ('ANN'), summer ('DJF') and winter ('JJA'). For each time period and season the trends for each ocean sector are plotted with the specific time period labelled below. Bold symbols indicate significant trends (significance indicates that the ensemble mean trend is larger than the inter-model standard deviation). Before calculating trends, the period 1900–2005 (taken from historical simulations) and the period 2006–2099 (taken from the RCP projections) were joined into a continuous time series.

RCP scenarios. However, the winter trends are not significant in any sector or time period (Figure 7a), which is probably a consequence of the fact that the winter time-mean surface jet is wider and more difficult to define. In particular, there is a double jet structure over the Pacific sector (Figure 8), which makes it difficult to unambiguously identify a sub-polar jet in some models. In the annual mean and summer season the poleward jet shifts are largest over the Atlantic sector and smallest over the Indian sector.

[19] The characteristics of the ensemble mean 20th and 21st century changes in jet strength vary considerably across the ocean sectors (Figures 9 and 10). In all sectors the increases approximately reflect the radiative forcing scenarios, with stabilisation by 2100 in RCP4.5 and continued increases through 2100 in RCP8.5. Over the Pacific sector the simulated linear trends for the period 2050–2098 following RCP8.5 are dramatic (0.15 m s^{-1} decade^{-1}), about double the trends seen over the Atlantic (0.07 m s^{-1} decade^{-1}) and Indian (0.07 m s^{-1} decade^{-1}) sectors. The increases in winter (JJA) are also consistent with radiative forcing by GHGs, but with the strongest response over the Indian sector (Figure 9c, f). Again, the response over the Atlantic sector is considerably weaker and the trend is not significant in any of the periods considered. As was seen in the jet position diagnostics, the periods of ozone depletion and recovery are clearly evident in the summer season (DJF) (Figure 9b, e). Over the historical period there is a distinct increase in strength over the period 1960–1999 in the ensemble mean (Figure 10), which is consistent with the observed increases in polarity of the SAM over the same period [*Marshall*, 2003]. In the first half of the 21st century in summer (DJF) the changes are not significant in either the RCP4.5 or RCP8.5 simulations, whereas the winter (JJA) changes are significant over the Indian sector. This indicates that the stratospheric ozone recovery and GHG forcing responses approximately cancel in summer. In the second half of the 21st century the RCP8.5 scenario results in a period of further jet strengthening in both summer and winter as the rate of ozone recovery diminishes and GHG concentrations rapidly increase. As in the annual mean, the ensemble mean trend over the Pacific sector for RCP8.5 in summer is approximately twice as large as for the Atlantic sector.

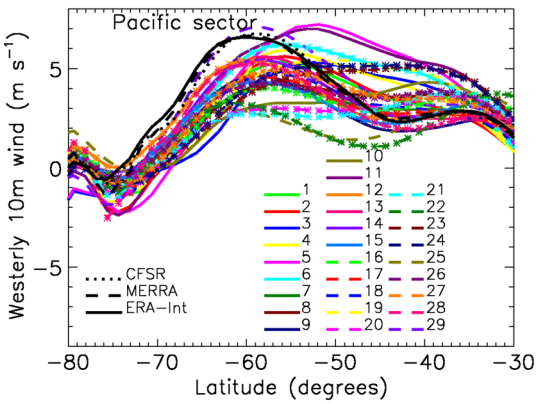

Figure 8. As in Figure 2d, but for winter (June–August).

3.4. High and Low-Top Models

[20] The projected changes documented in the previous section show a wide range of responses among the different models. Previous studies have shown clear differences in circulation response to GHG forcing when models with an upper boundary at or above 1 hPa ("high top" models) are compared to those with a lower-altitude "low top". Under increased GHG concentrations, a stronger increase in the Brewer Dobson circulation is seen in high top models, which cannot be captured in low-top models [*Scaife et al.*, 2012; *Karpechko and Manzini*, 2012]. *Scaife et al.* [2012] suggest that resulting differences in changes in vertical wind shear (and, by thermal wind balance, the meridional temperature gradients) at the tropopause influence the structure of baroclinic eddies in the troposphere [e.g. *Kushner et al.*, 2001; *Chen and Held*, 2007; *Wittman et al.*, 2007; *Kidston et al.*, 2011] and consequently the strength and position of the tropospheric jet. Consistent with this, *Wilcox et al.* [2013] have shown that those CMIP5 models with a larger

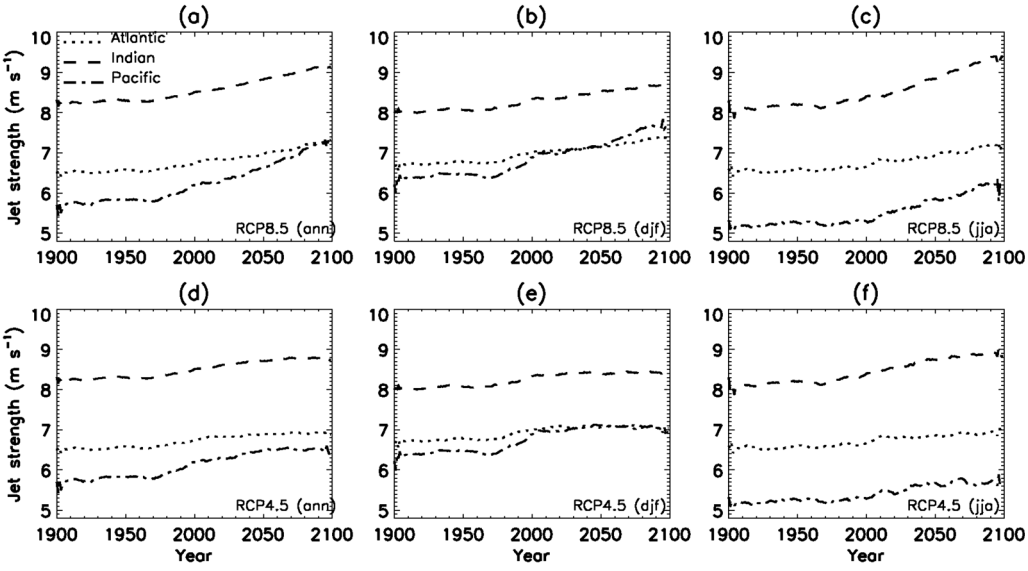

Figure 9. As in Figure 6 but for jet strength.

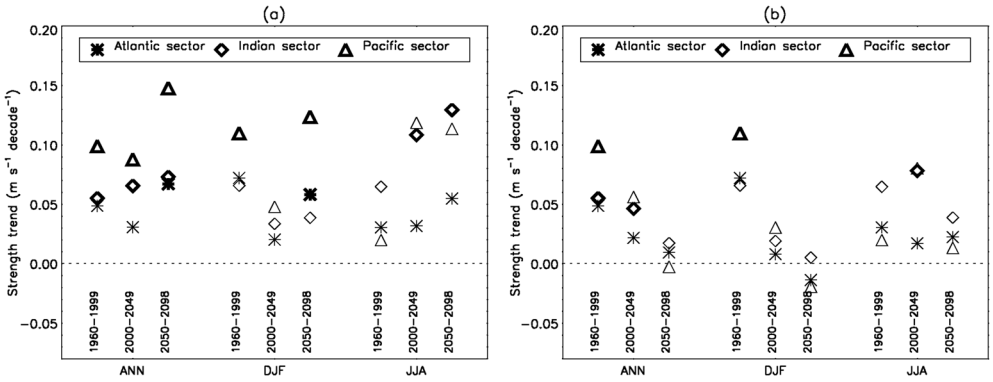

Figure 10. As in Figure 7 but for jet strength.

increase in their upper-level equator-to-pole summer temperature gradient also exhibit larger poleward shifts of the summer tropospheric jet at 500 hPa. We therefore now investigate whether there is a difference between the high and low top models in their projections of both position and strength of the surface jet across the Atlantic, Indian and Pacific sectors.

[21] The results show that on average the high top models exhibit a larger equatorward bias in present-day annual-mean jet position and a larger 21st century poleward shift (blue stars in Figure 11) compared to low top models (red crosses in Figure 11). This difference is nominally statistically significant at the 5% level over the Pacific sector (1.5°, $p = 0.03$). However, it should be noted that of the high top models with large biases and shifts, two closely related model groups, 20–21–22 and 23–24, could be considered as single models. When taking this into consideration the difference is no longer statistically significant (0.7°, $p = 0.13$).

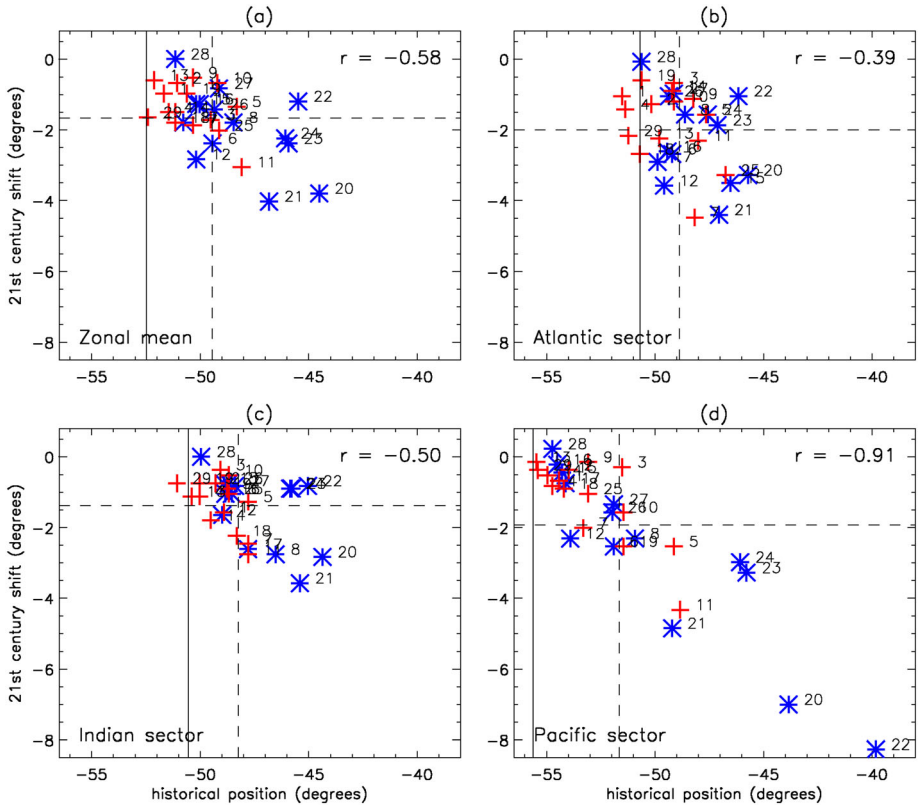

Figure 11. (a) Scatter plot of historical annual mean surface jet position versus 21st century change in the CMIP5 models. (b), (c) and (d) show the same but for the Atlantic, Indian and Pacific sectors, respectively. For the CMIP5 model results the mean over period 1960–1999 is used for the historical time slice and the mean over the period 2059–2098 is used for the future time slice, which is taken from the RCP8.5 scenario. The blue stars indicate high top models and the red plus signs indicate low top models. The solid vertical line shows the jet position calculated from ERA-Interim over the period 1979–1999. The vertical dashed line shows the CMIP5 historical ensemble mean and the horizontal dashed line shows the ensemble mean change. The correlations are shown in the top right-hand corner of each plot.

Similarly, in terms of annual-mean jet strength a few high top models show larger change but overall high-top/low-top differences were found to be small in terms of present-day bias or projected 21st century change (not shown).

[22] Consistent with analysis of the DJF zonal mean jet position conducted by *Wilcox et al*. [2013], we find that high/low top differences in jet shift are linked primarily to differences in tropical upper-tropospheric temperature change, which appear to influence the surface jet by altering the upper-level meridional temperature gradient (following *Wilcox et al*. [2013] we define this as the difference between temperature at 250 hPa between 25°S and 0° and temperature at 150 hPa between 90°S and 75°S). This is seen in inter-model correlations between jet shift and tropical temperature change, which are significant across the ocean sectors (Table 3). However, correlations between jet shift and polar temperature change are insignificant over the Indian and Pacific sectors.

[23] More mixed results relating to high/low top differences in jet strength change are seen in Table 3, based on 21st century changes following the RCP8.5 scenario. Over the Atlantic sector the results are similar to those based on jet shift, whereby the high top models show a larger change that is significantly correlated with tropical warming (and the change in meridional temperature gradient). This can be contrasted with the Pacific and Indian sectors, where changes in strength are less strongly correlated with tropical temperature change (Table 3).

3.5. Jet Shift and State Dependence

[24] In addition to inter-model differences in tropical warming and stratospheric response, feedbacks within the troposphere are likely to be an important source of inter-model spread in projected jet shift. Such feedbacks have been used to explain state dependence in jet position, whereby larger future jet position changes are associated with models with larger present day jet position bias (Figure 11). A large negative correlation is clear in all basins and has already been highlighted in assessments of zonal mean diagnostics in previous coupled climate model comparisons [e.g. *Kidston and Gerber*, 2010]. The inter-model correlation between present-day position and projected 21st century change is −0.58 for the RCP8.5 scenario (Figure 11a). For comparison with *Kidston and Gerber* [2010] we define 21st century change as differences as between 2059–2098 in the RCP8.5 scenario simulations and 1960–1999 in the historical simulations. For the zonal mean jet position we find similar correlations to *Kidston and Gerber* [2010], with the largest correlation in winter ($r = -0.91$), a weak correlation in summer ($r = -0.23$) and strong correlations in autumn and spring (Table 4). However, this state dependence is not consistently evident in annual mean jet position across the different ocean sectors. Over the Atlantic sector the correlation is relatively weak ($r = -0.39$) compared with the correlations over the Indian sector ($r = -0.50$) and Pacific sector ($r = -0.91$). The Pacific sector gives the strongest correlations in autumn, winter and spring and all sectors show weak correlations in summer. The weak spring and winter correlations over the Atlantic are conditional on omitting model 28 (MRI-CGCM3), which is an influential outlier due to jumps between two maxima in westerly wind (which is indicated in the annual mean shown in Figure 2b). For jet strength the state dependence is generally weaker than for position (Table 4). The only significant correlation occurs over the Indian sector in winter ($r = -0.49$).

[25] The zonally varying state dependence characteristics raise the question of whether different mechanisms might

Table 3. Correlations Between Northward Change in Annual Mean Surface Jet Position and Change in Annual Mean Temperature Following the RCP8.5 Scenario[a]

	Zonal Mean		Atlantic Sector		Indian Sector		Pacific Sector	
	Position	Strength	Position	Strength	Position	Strength	Position	Strength
Tropical-polar	**−0.73**	**0.57**	**−0.77**	**0.65**	**−0.56**	0.36	**−0.26** **(−0.52*)**	**0.59**
Tropical	**−0.58**	**0.49**	**−0.58**	**0.80**	**−0.64**	0.29	**−0.38**	**0.46**
Polar	**0.56**	**−0.38**	**0.60**	−0.14	0.24	−0.28	0.02	**−0.45**

[a]Here the tropical temperature is defined as the zonal or sector mean at 250 hPa between 25°S and 0° and the polar temperature is defined at 150 hPa between 90°S and 75°S. The changes are defined as time slice difference between the periods 2059–2098 in the RCP8.5 scenario and 1960–1999 in the historical forcing simulations. Bold indicates significance at the 5% level based on a two-tailed test. The asterisk indicates a correlation coefficient with model 22 omitted.

Table 4. Correlations Between Present-day Mean and Projected 21st Century Change in Jet Position and Strength[a]

	Zonal Mean		Atlantic Sector		Indian Sector		Pacific sector	
	Position	Strength	Position	Strength	Position	Strength	Position	Strength
ANN	**−0.58**	−0.04	**−0.39**	0.00	**−0.50**	−0.13	**−0.91**	−0.04
DJF	−0.23	−0.08	−0.29	−0.00	−0.24	0.01	−0.29	−0.19
MAM	**−0.54**	−0.14	−0.26	0.04	**−0.55**	−0.20	**−0.63**	−0.20
JJA	**−0.91**	−0.11	−0.60 (−0.21*)	−0.17	**−0.79**	**−0.49**	**−0.90**	0.30
SON	**−0.70**	−0.03	**−0.58** **(−0.41*)**	−0.20	−0.40	−0.06	**−0.67**	0.09

[a]Here the zonal mean, Atlantic, Indian and Pacific sectors are shown for annual mean (ANN) and all four seasons. The changes are defined as time slice difference between the periods 2059–2098 in the RCP8.5 scenario and 1960–1999 in the historical forcing simulations. Bold indicates significance at the 5% level based on a two-tailed test. The asterisks indicate correlations with model 28 omitted.

be responsible for the surface jet changes in different ocean sectors detailed above. Inter-basin differences in the time mean structure of the Southern Hemisphere westerly wind field further emphasis this point. These differences are clearest between the Atlantic and Pacific sectors, which are therefore the focus of comparisons here. Over the Indian sector (not shown) and Pacific sector (Figure 12), ERA-Interim shows a clear sub-tropical jet (at ~30°S and ~200 hPa) and a clear lower-tropospheric sub-polar jet at ~50°S. However, over the Atlantic sector (Figure 13) ERA-Interim exhibits nearly merged sub-polar and sub-tropical jets. Here agreement with the CMIP5 models is relatively good in the sense that they also exhibit nearly merged jets. However, over the Pacific sector the CMIP5 models exhibit a wide range of structures, with some models successfully capturing the distinct sub-polar and sub-tropical jets and others showing much more merged structures (Figure 12).

[26] To investigate the implications of these differences in structure, simple indices based on two suggested mechanisms for state dependence in jet position are considered. These mechanisms, put forward by *Barnes and Hartmann* [2010] and *Simpson et al*. [2012], both relate shifts in the jet to tropospheric eddy feedbacks that depend on the time mean jet structure. *Barnes and Hartmann* [2010] suggest that differences in eddy feedback could originate from differences in wave breaking on the poleward side of the sub-polar jet. According to this mechanism a poleward shift occurs when poleward breaking is suppressed and the resulting wider jet extends to higher latitudes. The implication is that models with jets that already exhibit weak poleward

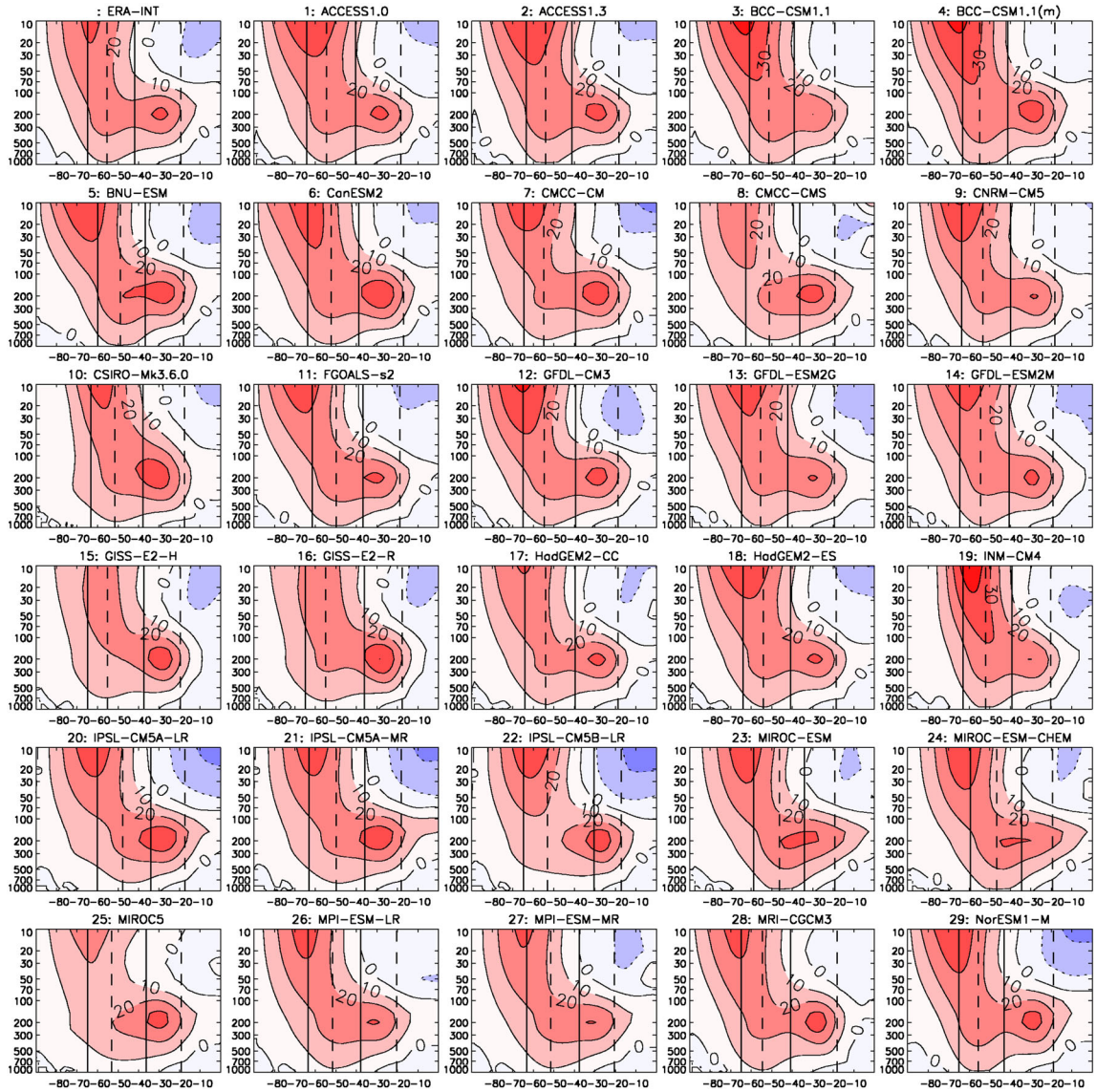

Figure 12. Pacific sector annual mean westerly wind climatology from ERA-Interim and CMIP5 models. For the CMIP5 models output from the historical runs was used, averaged over the period 1985–2004. For ERA-Interim data were averaged over the period 1985–2004. The vertical dashed lines define the latitude range of the PT-distance diagnostic and the vertical solid lines define the latitude range of the *P*-width distance diagnostic (see text for details). Contour intervals are $10\,m\,s^{-1}$ with negative contours indicated by dotted lines.

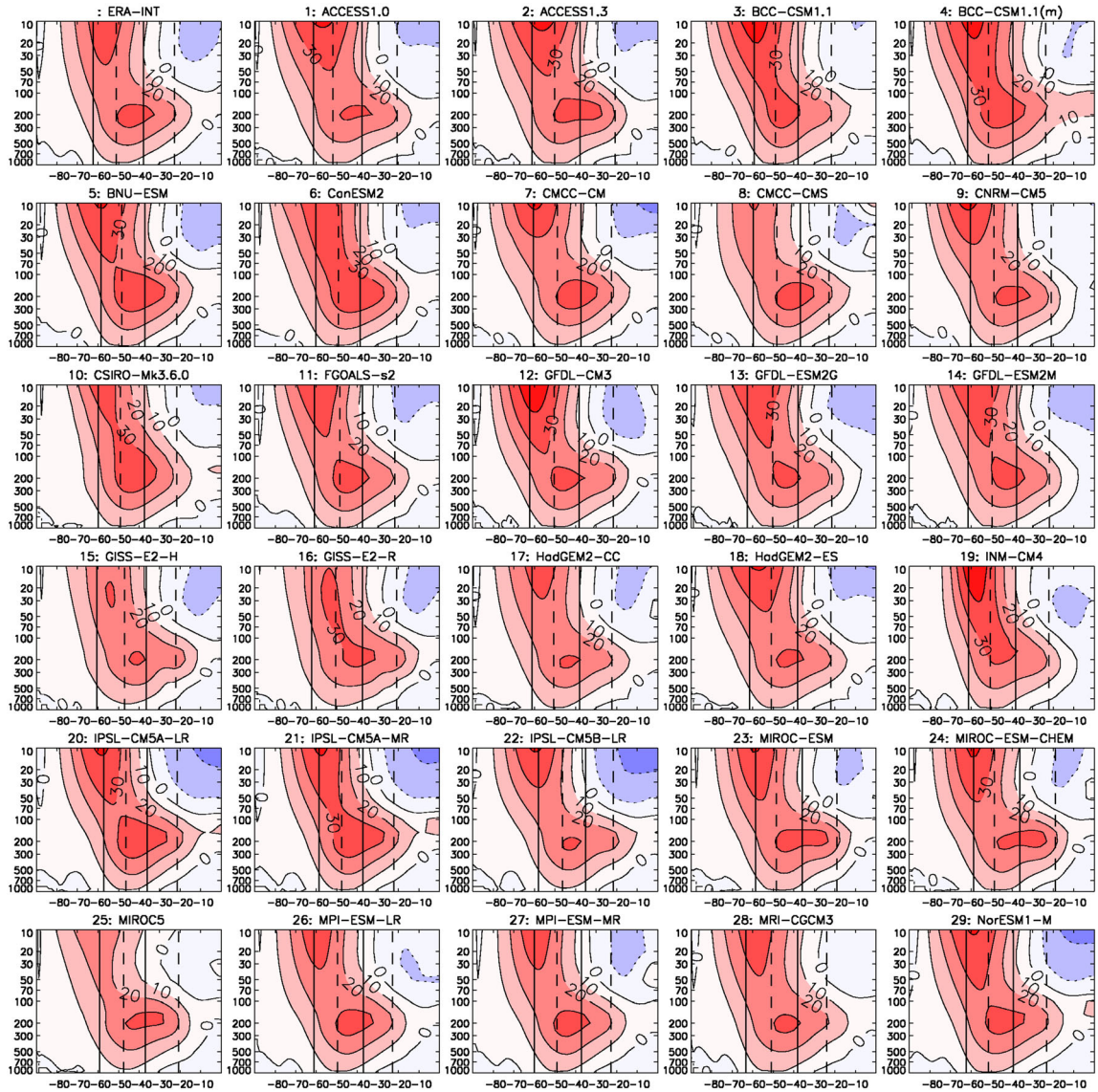

Figure 13. As in Figure 12, but for the Atlantic sector.

wave breaking (and a wider, more poleward, structure) show weak shifts under global warming, since wave breaking is already suppressed in those models. An alternative mechanism relating to eddy feedbacks on the equatorward side of the jet was suggested by *Simpson et al*. [2012], who show that the tropospheric eddy feedback (and poleward shift) is stronger when the distance between the sub-polar eddy-driven jet and the sub-tropical critical line is smaller. Higher latitude jets with a larger distance exhibit a weaker poleward jet shift due to a weaker latitudinal coherence of eddy momentum flux convergence across the phase speed spectrum. Their results are for a specific case of tropical stratospheric heating in a simplified GCM (sGCM), but may be relevant more generally.

[27] Simple indices were defined to assess consistency with these theories. Indices of the distance between the sub-polar jet and the sub-tropical critical line (PT-distance) and the width of sub-polar jet itself (*P*-width) were defined based on *Simpson et al*. [2012] and *Barnes and Hartmann* [2010], respectively. The PT-distance is defined as the distance between the surface jet position (i.e. the maximum in 10 m westerly wind) and the latitude of the $10\,m\,s^{-1}$ contour at 400 hPa on the equatorward side of the Southern Hemisphere sub-tropical jet. A threshold of $10\,m\,s^{-1}$ was used since this approximately defines the equatorward limit of critical lines associated with the important eddy feedbacks in the model used by *Simpson et al*. [2012] (similar results were found using a smaller threshold of $5\,m\,s^{-1}$). The 400 hPa level was used by *Simpson et al*. [2012], since the main eddy feedbacks occur at this height in the sGCM that they used. Both latitudes for each model and sector are marked by vertical dashed lines in Figures 12 and 13.

[28] Over the Indian and Pacific sectors the historical PT-distance is dominated by the sub-polar jet position and therefore correlations with surface jet shift largely mirror the results seen for the sub-polar jet position alone (Figure 14). However, over the Atlantic sector the sub-tropical component of the PT-distance varies significantly. In fact variations in the sub-tropical and sub-polar components of the PT-distance are significantly correlated across the different

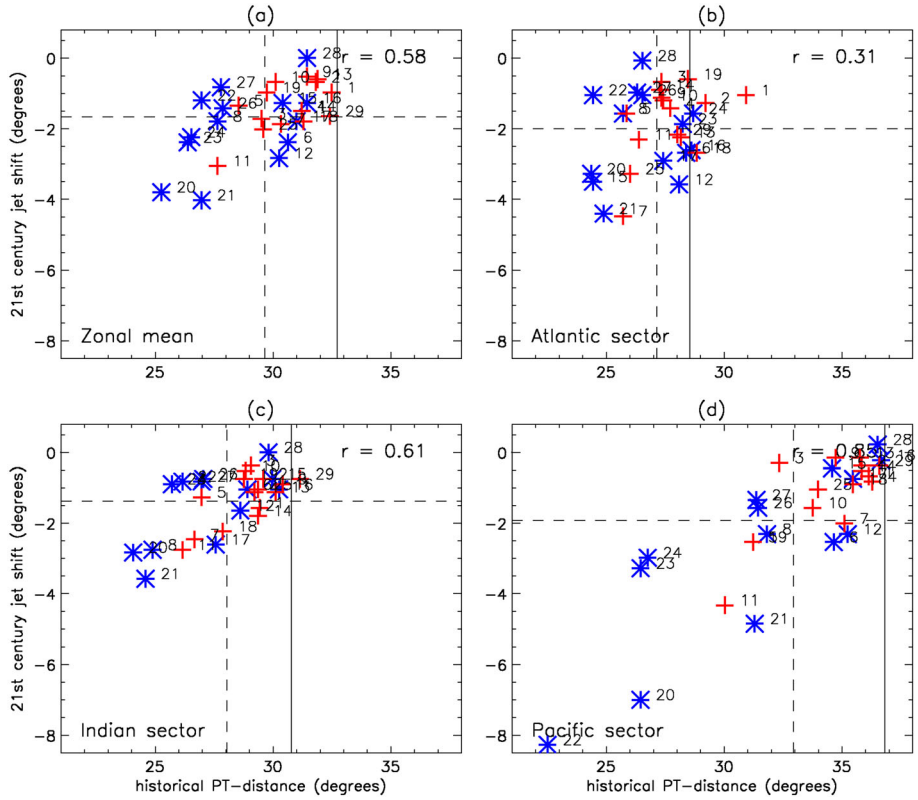

Figure 14. As in Figure 11, but showing historical PT-distance along the *x*-axis.

models ($r = 0.38$). This contrasts with the Indian and Pacific sectors where there is no significant correlation ($r = -0.06$ and $r = 0.25$, respectively). The implication of this is that inter-model differences in jet position over the Atlantic sector are more closely associated with latitudinal displacements of the merged jet structure and differences in PT-distance are smaller. The mechanism of *Simpson et al.* [2012] would not therefore be expected to give significant state dependence over the Atlantic sector.

[29] For *P*-width the results are rather different. The *P*-width index is calculated from the time mean 10-m westerly wind field and defined as the meridional distance between latitudes where the westerly wind is half the value of the jet-core maximum. This therefore is a measure of the shape of the sub-polar jet only and is not explicitly related to the sub-tropical jet. In Figure 15 it can be seen that correlations between historical *P*-width and projected jet shift are positive over the Atlantic and Indian sectors ($r = 0.19$ and $r = 0.34$, respectively), but negative over the Pacific sector ($r = -0.53$). Although not significant, the positive sign of the correlations over the Atlantic and Indian sectors is consistent with the predictions of *Barnes and Hartmann* [2010], i.e. wider jets show smaller shifts.

[30] The implications of this analysis are that over the Atlantic and Indian sectors the correlations indicate a role for the mechanisms suggested by both *Barnes and Hartmann* [2010] and *Simpson et al.* [2012], whereas over the Pacific sector they are more consistent with *Simpson et al.* [2012]. More broadly, the different westerly wind structures and correlation results emphasise that the dynamics of the jet response seem to differ across different sectors of the Southern Ocean.

4. Discussion and Conclusions

[31] In this paper an assessment of the CMIP5 models' simulation of near-surface (10 m) westerly winds over the Southern Ocean (the surface jet) is presented. Their skill at simulating both the surface jet and its response to future forcing scenarios is assessed. In addition to zonal mean diagnostics, the Atlantic, Indian and Pacific sectors are considered with the aim of characterising zonal asymmetries in bias and response.

[32] An equatorward bias in the present-day zonal mean surface jet position was found to occur in many of the CMIP5 models (ensemble mean of 3.3° in latitude). Indeed none of the models assessed here exhibit a surface jet that is poleward of that derived from any of three contemporary reanalysis datasets (CFSR, ERA-Interim or MERRA). The zonal mean bias is mainly associated with biases over the Indian and Pacific sectors with the exception being the Atlantic sector, for which the ensemble mean equatorward bias is much smaller (1.4° in latitude). In terms of the zonal mean surface jet, *Wilcox et al.* [2013] and *Swart and Fyfe* [2012] also found a position bias in most of the CMIP5 models. It is therefore apparent that the equatorward jet position bias that was seen in many of the CMIP3 models [*Kidston and Gerber*, 2010; *Son et al.*, 2010; *Swart and Fyfe*, 2011] is still a key issue in the CMIP5 multi-model ensemble.

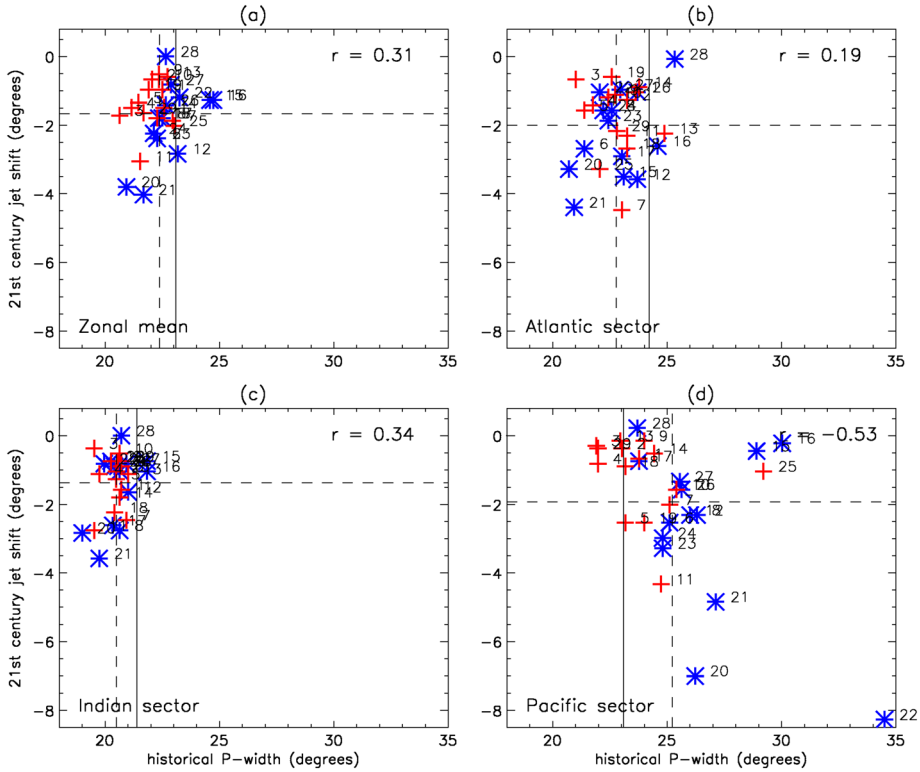

Figure 15. As in Figure 11, but showing historical *P*-width along the x-axis.

[33] The ensemble mean bias in the position of the jet in a subset of nine available atmosphere-only AMIP simulations was found to be 28% smaller than the historical CMIP5 simulations with corresponding atmospheric models. This comparison suggests that an important contributor to the CMIP5 bias is in coupling to the ocean and sea ice models, which can amplify atmospheric biases and introduce biases generated by the ocean/ice models themselves or by the coupling procedure. We note that it is important to understand the origin of surface jet biases to assess the robustness of the atmospheric response in climate change scenarios, but we leave further analysis for a future study.

[34] There is a clear zonal asymmetry in the response of the surface jet over the 21st century following the RCP8.5 high emissions scenario. This is most apparent in jet strength. For annual mean strength trends over the period 2050–2098 the response over the Pacific is very large ($0.15\,m\,s^{-1}$ (2.4%) $decade^{-1}$) and approximately double that of the Atlantic ($0.07\,m\,s^{-1}$ (1.1%) $decade^{-1}$) and Indian ($0.07\,m\,s^{-1}$ (0.8%) $decade^{-1}$) sectors (percentages are relative to the ensemble mean jet strength at 2050). In terms of annual mean jet position over the same period and scenario the ensemble mean poleward shift is largest over the Atlantic sector (0.33° $decade^{-1}$), followed by the Pacific (0.28° $decade^{-1}$) and Indian (0.18° $decade^{-1}$) sectors. This is consistent with previous assessments of Southern Hemisphere circulation response to GHG forcing [*Brandefelt and Kallen*, 2004; *Arblaster and Meehl*, 2006], although a quantitative comparison is not possible since these studies do not show jet strength and position diagnostics. We found three phases in atmospheric jet shift and strength: a poleward shift and strengthening over the latter period of the 20th century; a plateau in the first half of the 21st century during the period of most rapid stratospheric ozone recovery; and a shift and strengthening more or less pronounced in the second half of the 21st century depending on the intensity of the radiative forcing. The reduced jet shift and reduced strengthening in the first half of the 21st century occurs mainly in the summer season, which is the season of strongest influence of stratospheric ozone recovery and therefore strongest offset of the year-round influence of projected GHG increases. This summer offset represents an approximate cancellation between these two influences on surface jet shift, which is in agreement with previous findings based on other models and model inter-comparisons [*Son et al.*, 2010; *Arblaster et al.*, 2011; *Polvani et al.*, 2011] and other definitions of jet position in the CMIP5 models [*Wilcox et al.*, 2013]. An implication of this cancellation is that ocean sectors with a larger sensitivity in terms of jet position to GHG increases also have a larger sensitivity to stratospheric ozone recovery.

[35] To investigate the causes of the large spread in projected jet shifts, the possible role of the height of model tops in the CMIP5 models was assessed. It was found that on average high and low top models exhibit different 21st century changes in annual mean jet position. Consistent with the analysis of the summer season zonal mean jet position of *Wilcox et al.* [2013], stronger responses in annual mean jet position in the high top models were found across all sectors. The results suggest that this is linked to stronger upper-tropospheric tropical warming (and therefore stronger increases in upper-level equator-to-pole temperature difference) in the high top models (as found by *Wilcox et al.* [2013]). In contrast to the findings for jet position, high/low top model differences in 21st century changes in annual mean jet strength were found to be small over the Indian and Pacific sectors. Here, inter-model correlations between jet

strength change and tropical temperature change are weak and the polar component of changes in upper-level meridional temperature gradient is more important. This further emphasises the role of tropical upper-tropospheric warming in high/low top differences. However, since the CMIP5 models differ in many ways other than model top, it is not possible to directly attribute the differences between the high and low top subsets to the height of the model lid. In particular, *Santer et al*. [2012] recently identified inter-model differences in the treatment of ozone (e.g. see Table 1) as a key influence on lower-stratospheric temperature trends in the CMIP5 models.

[36] In addition to inter-model differences in tropical upper-tropospheric warming and stratospheric response, the theoretical implications of differences in historical mean-state tropospheric jet structure for projected jet shift were investigated. An inter-model relationship between present-day mean-state bias and projected 21st century change (state dependence) was found in annual mean zonal mean jet position with a correlation of $r = -0.58$. This is slightly smaller than the value obtained by *Wilcox et al*. [2013] ($r = -0.64$) based on their assessment of 500 hPa jet position in the CMIP5 models and smaller than the surface jet correlations found in the CMIP3 models by *Kidston and Gerber* [2010] ($r = -0.77$). The annual cycle of correlations is similar to that found by with *Kidston and Gerber* [2010], who used the same diagnostic based on near-surface wind. When the above analysis was extended to individual ocean sectors, it was found that correlations are even stronger over the Pacific sector ($r = -0.91$), but weaker over the Atlantic sector ($r = -0.39$).

[37] The variations in state dependence reflect significant differences in mean state structure across the different sectors and help provide some insight into mechanisms for projected shifts of the jet. The differences in structure were captured with simple indices of the sub-polar jet width (*P*-width) and the distance between the sub-polar and sub-tropical jet (PT-distance), which are related to mechanisms for state dependence suggested by *Barnes and Hartmann* [2010] and *Simpson et al*. [2012], respectively. The clearest differences are between the Atlantic and Pacific sectors. Over the Atlantic sector the reanalysis and models show a consistent merged jet structure, with no clear separation between the sub-polar and sub-tropical jets (i.e. small PT-distance). Here projected jet shifts are not significantly correlated with either *P*-width ($r = 0.19$) or PT-distance ($r = 0.31$). In contrast over the Pacific sector the CMIP5 models exhibit a wide range of structures, with some models successfully capturing the distinct sub-polar and sub-tropical jets seen in the re-analyses and others showing much more merged structures. Inter-model correlations with projected shifts are much larger for PT-distance ($r = 0.85$) than *P*-width ($r = -0.28$ with outlier model 22 excluded). The implication of these results is that different dynamical regimes in the different ocean sectors lead to contrasting mechanisms for projected jet shift. The extent to which the above mechanisms emerge in full GCMs is not proven here and consistency with these and other theories across the different sectors would require further diagnostics relating to baroclinic eddy life cycles and length scales [*Wittman et al*., 2007; *Kidston et al*., 2011], internal jet variability [*Kidston and Gerber*, 2010; *Barnes and Hartmann*, 2012] and phase speed [*Chen and Held*, 2007; *Simpson et al*., 2012]. It is anticipated that a more comprehensive understanding of jet bias and shift across the Southern Ocean may be possible by not only considering the zonal mean, but focussing on sectors across individual ocean basins.

[38] **Acknowledgments.** This study is part of the British Antarctic Survey Polar Science for Planet Earth Programme. It was funded by The UK Natural Environment Research Council (grant reference number NE/J005339/1). Three anonymous reviewers are thanked for their comments and suggestions, which helped to significantly improve the manuscript. We acknowledge the World Climate Research Programme's Working Group on Coupled Modelling, which is responsible for CMIP, and we thank the climate modeling groups for producing and making available their model output (listed in Table 1 of this paper). For CMIP the U.S. Department of Energy's Program for Climate Model Diagnosis and Intercomparison provides coordinating support and led development of software infrastructure in partnership with the Global Organization for Earth System Science Portals. The European Centre for Medium Range Weather Forecasting are thanked for providing the ERA-40 and ERA-Interim datasets. The Global Modeling and Assimilation Office (GMAO) and the GES DISC are acknowledged for the dissemination of the MERRA dataset. The CFSR data was retrieved from the Research Data Archive, which is managed by the Data Support Section of the Computational and Information Systems Laboratory at the National Center for Atmospheric Research in Boulder, Colorado.

References

Arblaster, J. M., and G. A. Meehl (2006), Contributions of external forcings to southern annular mode trends, *J. Clim.*, *19*(12), 2896–2905, doi:10.1175/JCLI3774.1.

Arblaster, J. M., G. A. Meehl, and D. J. Karoly (2011), Future climate change in the Southern Hemisphere: Competing effects of ozone and greenhouse gases, *Geophys. Res. Lett.*, *38*, L02701, doi:10.1029/2010gl045384.

Barnes, E. A., and D. L. Hartmann (2010), Testing a theory for the effect of latitude on the persistence of eddy-driven jets using CMIP3 simulations, *Geophys. Res. Lett.*, *37*, L15801, doi:10.1029/2010gl044144.

Barnes, E. A., and D. L. Hartmann (2012), Detection of Rossby wave breaking and its response to shifts of the midlatitude jet with climate change, *J. Geophys. Res.*, *117*(D9), D09117, doi:10.1029/2012jd017469.

Bracegirdle, T. J., and G. J. Marshall (2012), The reliability of Antarctic tropospheric pressure and temperature in the latest global reanalyses, *J. Clim.*, *25*, 7138–7146, doi:10.1175/JCLI-D-11-00685.1.

Bracegirdle, T. J., W. M. Connolley, and J. Turner (2008), Antarctic climate change over the twenty first century, *J. Geophys. Res. Atmos.*, *113*(D3), doi:10.1029/2007jd008933.

Brandefelt, J., and E. Kallen (2004), The response of the Southern Hemisphere atmospheric circulation to an enhanced greenhouse gas forcing, *J. Clim.*, *17*(22), 4425–4442, doi:10.1175/3221.1.

Bromwich, D. H., J. P. Nicolas, and A. J. Monaghan (2011), An Assessment of Precipitation Changes over Antarctica and the Southern Ocean since 1989 in Contemporary Global Reanalyses, *J. Clim.*, *24*(16), 4189–4209, doi:10.1175/2011jcli4074.1.

Chen, G., and I. M. Held (2007), Phase speed spectra and the recent poleward shift of Southern Hemisphere surface westerlies, *Geophys. Res. Lett.*, *34*(21), L21805, doi:10.1029/2007gl031200.

Ciasto, L. M., and D. W. J. Thompson (2008), Observations of large-scale ocean-atmosphere interaction in the southern hemisphere, *J. Clim.*, *21*(6), 1244–1259, doi:10.1175/2007jcl11809.1.

Cionni, I., V. Eyring, J. F. Lamarque, W. J. Randel, D. S. Stevenson, F. Wu, G. E. Bodeker, T. G. Shepherd, D. T. Shindell, and D. W. Waugh (2011), Ozone database in support of CMIP5 simulations: results and corresponding radiative forcing, *Atmos. Chem. Phys.*, *11*(21), 11267–11292, doi:10.5194/acp-11-11267-2011.

Dee, D. P., et al. (2011), The ERA-Interim reanalysis: configuration and performance of the data assimilation system, *Q. J. R. Meteorolog. Soc.*, *137*(656), 553–597, doi:10.1002/qj.828.

Fyfe, J. C., and O. A. Saenko (2006), Simulated changes in the extratropical Southern Hemisphere winds and currents, *Geophys. Res. Lett.*, *33*, L06701, doi:10.1029/2005GL025332.

Guemas, V., and F. Codron (2011), Differing Impacts of Resolution Changes in Latitude and Longitude on the Midlatitudes in the LMDZ Atmospheric GCM, *J. Clim.*, *24*(22), 5831–5849, doi:10.1175/2011jcli4093.1.

Hall, A., and M. Visbeck (2002), Synchronous variability in the Southern Hemisphere atmosphere, sea ice, and ocean resulting from the Annular Mode, *J. Clim.*, *15*, 3043–3057, doi:10.1175/1520-0442(2002)015<3043:SVITSH>2.0.CO;2.

Hoskins, B. J., and K. I. Hodges (2005), A New Perspective on Southern Hemisphere Storm Tracks, *J. Clim.*, *18*, 4108–4129, doi:10.1175/JCLI3570.1.

Hourdin, F., et al. (2012), Impact of the LMDZ atmospheric grid configuration on the climate and sensitivity of the IPSL-CM5A coupled model, *Clim. Dyn.*, doi:10.1007/s00382-012-1411-3.

Hurrell, J. W., J. J. Hack, D. Shea, J. M. Caron, and J. Rosinski (2008), A new sea surface temperature and sea ice boundary dataset for the Community Atmosphere Model, *J. Clim.*, *21*(19), 5145–5153, doi:10.1175/2008jcli2292.1.

Inatsu, M., and B. J. Hoskins (2004), The zonal asymmetry of the Southern Hemisphere winter storm track, *J. Clim.*, *17*(24), 4882–4892, doi:10.1175/jcli-3232.1.

Karpechko, A. Y., and E. Manzini (2012), Stratospheric influence on tropospheric climate change in the Northern Hemisphere, *J. Geophys. Res. Atmos.*, *117*, D05133, doi:10.1029/2011jd017036.

Karpechko, A. Y., N. P. Gillett, G. J. Marshall, and A. Scaife (2008), Stratospheric influence on circulation changes in the Southern Hemisphere troposphere in coupled climate models, *Geophys. Res. Lett.*, *35*(20), L20806, doi:10.1029/2008gl035354.

Kawase, H., T. Nagashima, K. Sudo, and T. Nozawa (2011), Future changes in tropospheric ozone under Representative Concentration Pathways (RCPs), *Geophys. Res. Lett.*, *38*, L05801, doi:10.1029/2010gl046402.

Kent, E. C., S. Fangohr, and D. I. Berry (2013), A comparative assessment of monthly mean wind speed products over the global ocean, *Int. J. Climatol.*, in press, doi:10.1002/joc.3606.

Kidston, J., and E. P. Gerber (2010), Intermodel variability of the poleward shift of the austral jet stream in the CMIP3 integrations linked to biases in 20th century climatology, *Geophys. Res. Lett.*, *37*, L09708, doi:10.1029/2010gl042873.

Kidston, J., G. K. Vallis, S. M. Dean, and J. A. Renwick (2011), Can the Increase in the Eddy Length Scale under Global Warming Cause the Poleward Shift of the Jet Streams?, *J. Clim.*, *24*(14), 3764–3780, doi:10.1175/2010jcli3738.1.

Kushner, P. J., I. M. Held, and T. L. Delworth (2001), Southern Hemisphere atmospheric circulation response to global warming, *J. Clim.*, *14*, 2238–2249, doi:10.1175/1520-0442(2001)014<0001:SHACRT>2.0.CO;2.

Lamarque, J.-F., G. P. Kyle, M. Meinshausen, K. Riahi, S. J. Smith, D. P. van Vuuren, A. J. Conley, and F. Vitt (2011), Global and regional evolution of short-lived radiatively active gases and aerosols in the Representative Concentration Pathways, *Clim. Chang.*, *109*(1-2), 191–212, doi:10.1007/s10584-011-0155-0.

Le Quere, C., et al. (2007), Saturation of the Southern Ocean CO2 Sink Due to Recent Climate Change, *Science*, *316*(5832), 1735–1738, doi:10.1126/science.1136188.

Lovenduski, N. S., and N. Gruber (2005), Impact of the Southern Annular Mode on Southern Ocean circulation and biology, *Geophys. Res. Lett.*, *32*(11), L11603, doi:10.1029/2005gl022727.

Lovenduski, N. S., N. Gruber, S. C. Doney, and I. D. Lima (2007), Enhanced CO(2) outgassing in the Southern Ocean from a positive phase of the Southern Annular Mode, *Global Biogeochem. Cycles*, *21*(2), Gb2026, doi:10.1029/2006gb002900.

Maloney, E. D., and D. B. Chelton (2006), An assessment of the sea surface temperature influence on surface wind stress in numerical weather prediction and climate models, *J. Clim.*, *19*(12), 2743–2762, doi:10.1175/jcli3728.1.

Marshall, G. J. (2003), Trends in the Southern Annular Mode from observations and reanalyses, *J. Clim.*, *16*, 4134–4143, doi:10.1175/1520-0442(2003)016<4134:TITSAM>2.0.CO;2.

Meinshausen, M., et al. (2011), The RCP greenhouse gas concentrations and their extensions from 1765 to 2300, *Clim. Chang.*, *109*(1-2), 213–241, doi:10.1007/s10584-011-0156-z.

Meredith, M. P., and A. M. Hogg (2006), Circumpolar response of Southern Ocean eddy activity to a change in the Southern Annular Mode, *Geophys. Res. Lett.*, *33*(16), L16608, doi:10.1029/2006gl026499.

Miller, R. L., G. A. Schmidt, and D. T. Shindell (2006), Forced annular variations in the 20th century Intergovernmental Panel on Climate Change Fourth Assessment Report models, *J. Geophys. Res.*, *111*, 10.1029/2005JD006323.

Polvani, L. M., M. Previdi, and C. Deser (2011), Large cancellation, due to ozone recovery, of future Southern Hemisphere atmospheric circulation trends, *Geophys. Res. Lett.*, *38*, L04707, doi:10.1029/2011gl046712.

Randel, W. J., and F. Wu (2007), A stratospheric ozone profile data set for 1979–2005: Variability, trends, and comparisons with column ozone data, *J. Geophys. Res. Atmos.*, *112*(D6), D06313, doi:10.1029/2006jd007339.

Rienecker, M. M., et al. (2011), MERRA: NASA's Modern-Era Retrospective Analysis for Research and Applications, *J. Clim.*, *24*(14), 3624–3648, doi:10.1175/jcli-d-11-00015.1.

Roscoe, H. K., and J. D. Haigh (2007), Influences of ozone depletion, the solar cycle and the QBO on the Southern Annular Mode, *Q. J. R. Meteorolog. Soc.*, *133*(628), 1855–1864, doi:10.1002/qj.153.

Saha, S., et al. (2010), The NCEP Climate Forecast System Reanalysis, *Bull. Am. Meteorol. Soc.*, *91*(8), 1015–1057, doi:10.1175/2010bams3001.1.

Sallee, J. B., K. Speer, and R. Morrow (2008), Response of the Antarctic Circumpolar Current to atmospheric variability, *J. Clim.*, *21*(12), 3020–3039, doi:10.1175/2007jcli1702.1.

Sallee, J. B., K. G. Speer, and S. R. Rintoul (2010), Zonally asymmetric response of the Southern Ocean mixed-layer depth to the Southern Annular Mode, *Nat. Geosci.*, *3*(4), 273–279, doi:10.1038/ngeo812.

Santer, B. D., et al. (2012), Identifying human influences on atmospheric temperature, *Proc. Natl. Acad. Sci.*, doi:10.1073/pnas.1210514109.

Scaife, A., et al. (2012), Climate change projections and stratosphere–troposphere interaction, *Clim. Dyn.*, *38*, 2089–2097, doi:10.1007/s00382-011-1080-7.

Sen Gupta, A., and M. H. England (2006), Coupled ocean-atmosphere-ice response to variations in the Southern Annular Mode, *J. Clim.*, *19*(18), 4457–4486, doi:10.1175/jcli3843.1.

Shindell, T., and G. A. Schmidt (2004), Southern Hemisphere climate response to ozone changes and greenhouse gas increases, *Geophys. Res. Lett.*, *31*, L18209, doi:10.1029/2004GL020724.

Simpson, I. R., M. Blackburn, J. D. Haigh, and S. N. Sparrow (2012), A mechanism for the effect of tropospheric jet structure on the annular mode-like response to stratospheric forcing, *J. Atmos. Sci.*, *69*, 2152–2170, doi:10.1175/JAS-D-11-0188.1.

Son, S. W., et al. (2010), Impact of stratospheric ozone on Southern Hemisphere circulation change: A multimodel assessment, *J. Geophys. Res. Atmos.*, *115*, D00M07, doi:10.1029/2010JD014271.

Stammerjohn, S. E., D. G. Martinson, R. C. Smith, X. Yuan, and D. Rind (2008), Trends in Antarctic annual sea ice retreat and advance and their relation to El Nino-Southern Oscillation and Southern Annular Mode variability, *J. Geophys. Res. Oceans*, *113*(C3), C03S90, doi:10.1029/2007jc004269.

Swart, N. C., and J. C. Fyfe (2011), Ocean carbon uptake and storage influenced by wind bias in global climate models, *Nat. Clim. Change*, *2*(1), 47–52, doi:10.1038/nclimate1289.

Swart, N. C., and J. C. Fyfe (2012), Observed and simulated changes in the Southern Hemisphere surface westerly wind-stress, *Geophys. Res. Lett.*, *39*(16), L16711, doi:10.1029/2012gl052810.

Taylor, K. E., D. Williamson, and F. Zwiers (2000), The sea surface temperature and sea-ice concentration boundary conditions for AMIP II simulations Rep. 60, 25 pp, Lawrence Livermore National Laboratory, California.

Taylor, K. E., R. J. Stouffer, and G. A. Meehl (2012), An Overview of CMIP5 and the Experiment Design, *Bull. Am. Meteorol. Soc.*, *93*, 485–498, doi:10.1175/bams-d-11-00094.1.

Thompson, D. W. J., and S. Solomon (2002), Interpretation of recent Southern Hemisphere climate change, *Science*, *296*, 895–899, doi:10.1126/science.1069270.

Thompson, D. W. J., S. Solomon, P. J. Kushner, M. H. England, K. M. Grise, and D. J. Karoly (2011), Signatures of the Antarctic ozone hole in Southern Hemisphere surface climate change, *Nat. Geosci.*, *4*(11), 741–749, doi:10.1038/ngeo1296.

Verdy, A., J. Marshall, and A. Czaja (2006), Sea surface temperature variability along the path of the antarctic circumpolar current, *J. Phys. Oceanogr.*, *36*(7), 1317–1331, doi:10.1175/jpo2913.1.

Wang, Y. H., and G. Magnusdottir (2011), Tropospheric Rossby Wave Breaking and the SAM, *J. Clim.*, *24*(8), 2134–2146, doi:10.1175/2010jcli4009.1.

Wang, Z., T. Kuhlbrodt, and M. P. Meredith (2011), On the response of the Antarctic Circumpolar Current transport to climate change in coupled climate models, *J. Geophys. Res.*, *116*, C08011, doi:10.1029/2010JC006757.

Wilcox, L. J., A. J. Charlton-Perez, and L. J. Gray (2013), Trends in Austral jet position in ensembles of high- and low-top CMIP5 models, *J. Geophys. Res.*, *117*, D13115, doi:10.1029/2012JD017597.

Wittman, M. A. H., A. J. Charlton, and L. M. Polvani (2007), The effect of lower stratospheric shear on baroclinic instability, *J. Atmos. Sci.*, *64*(2), 479–496, doi:10.1175/jas3828.1.

Yang, X.-Y., R. X. Huang, and D. X. Wang (2007), Decadal changes of wind stress over the Southern Ocean associated with Antarctic ozone depletion, *J. Clim.*, *20*(14), 3395–3410, doi:10.1175/jcli4195.1.